

## Surfactant Charge Effects on the Location, Vibrational Spectra, and Relaxation Dynamics of Cyanoferrates in Reverse Micelles

Gerald M. Sando,<sup>†</sup> Kevin Dahl,<sup>‡</sup> and Jeffrey C. Owrutsky\*

Code 6111, U.S. Naval Research Laboratory, Washington, D.C. 20375-5342

Received: October 15, 2004; In Final Form: December 20, 2004

Ultrafast infrared spectroscopy has been used to measure vibrational energy relaxation (VER) and reorientation ( $T_r$ ) times for the high frequency CN stretches of potassium ferrocyanide and ferricyanide and the NO stretch of sodium nitroprusside (SNP) in several reverse micelle (RM) systems using cationic, anionic, and nonionic surfactants. The confinement effects on anion vibrational spectra and dynamics in aqueous RMs depend on the charge of the surfactant that is used to form the RMs. Spectra and VER dynamics of ferrocyanide are not significantly altered in the limited number of RMs in which it could be solubilized. The static spectra of ferricyanide suggest an environment that is most bulklike in anionic RMs and least bulklike in cationic RMs. The dynamics of ferricyanide are slower in cationic RMs and indistinguishable from the bulk in nonionic RMs. The VER dynamics and static spectra of SNP are indistinguishable from the bulk in anionic RMs, but much slower in cationic RMs. This suggests a strong surfactant–solute repulsion in the former and an attraction in the latter. Broad static spectra and probe frequency dependent dynamics are seen for SNP in nonionic RMs, indicating an inhomogeneous distribution of environments. Similar measurements were carried out for SNP in mixtures of water and a model compound containing only the hydrophilic portion of the nonionic surfactants in which RMs are not formed. The results closely resemble those observed for SNP in nonionic RMs and provide evidence that in the latter water penetrates the interface and hydrates the ethylene oxide groups before forming a water pool. The results are consistent with the explanation that Coulombic forces determine the anion location. The anions are repelled to the interior of the water pool, which has a bulklike environment in anionic RMs, and are attracted to the interface in cationic RMs, resulting in a strong interaction with the surfactant. The solute location in the nonionic RMs depends on the hydrophilic nature of the probe, with ferrocyanide and ferricyanide being more hydrophilic than SNP. These results and the dependence on surfactant charge are similar to those reported for azide.

### Introduction

Confined aqueous systems have received a great deal of attention in recent years due to the fundamental importance of aqueous confinement in biological systems.<sup>1–3</sup> Model confined aqueous systems have included nanoporous glasses as well as cyclodextrin cavities.<sup>4–10</sup> The use of reverse micelles (RMs) is a way of systematically controlling the extent of confinement. RMs consist of nanosized water droplets stabilized by surfactants that are formed in bulk organic solvents. In general, the size of RMs depends on the molar ratio of water to surfactant,  $\omega$ , where  $\omega = [\text{H}_2\text{O}]/[\text{surfactant}]$ . The monodisperse nature of RMs allows good control over the extent of confinement, with the radius of the RM often depending linearly on  $\omega$ . The size of the RM water pool or the corresponding hydrodynamic radii have been characterized for a wide variety of surfactant/solvent systems using dynamic light scattering, fluorescence quenching, and small-angle X-ray and neutron scattering and are generally on the order of tens of angstroms in diameter.<sup>11–20</sup> Previous studies of solutes in the water pool as well as the water pool itself have clearly established that the water pool is less polar and has less hydrogen bonding than bulk water. A blue shift of the O–H stretching frequencies<sup>21–24</sup> as well as

red shifts of the librational frequency<sup>25</sup> of water suggests a reduction in hydrogen bonding. A less polar solvation environment is suggested by a reduction in solvatochromatic shifts as compared to bulk water.<sup>26,27</sup> A layered water structure has been suggested by both experimental<sup>21–25,28,29</sup> and modeling studies.<sup>30–34</sup> The outer layer consists of water bound to surfactant headgroups,<sup>34</sup> followed by a restricted intermediate layer consisting of the next few nearest neighbors, and a bulklike interior region.

Previous time-resolved studies have demonstrated that dynamical processes in RMs often occur more slowly than in bulk water. These studies include solvation dynamics,<sup>35–38</sup> internal charge transfer,<sup>39–42</sup> isomerization,<sup>43,44</sup> dielectric relaxation,<sup>45,46</sup> and transient infrared spectroscopy.<sup>47–51</sup> These RMs can be made using cationic, anionic, or nonionic surfactants. There are reports in the literature in which spectral shifts and dynamics of probe species correlate with the surfactant charge, especially for charged solute species.<sup>35,36,52,53</sup> These observations have been related to the location of the probe within the RM interior and how it depends on surfactant charge. This behavior has been seen in studies of solvation dynamics where both static spectral shifts as well as effects on solvation dynamics depend little on  $\omega$  but differ significantly from the bulk behavior for oppositely charged probe and surfactant.<sup>35</sup> In this case, the probe resides in the interfacial region due to the Coulombic attraction between the probe and surfactant in an environment that changes little

\* To whom correspondence should be addressed. E-mail: jeff.owrutsky@nrl.navy.mil.

<sup>†</sup> NRL-ASEE Research Associate.

<sup>‡</sup> NRL-NRC Research Associate.

with  $\omega$ . A stronger  $\omega$  dependence was observed when the probe and surfactant have the same charge and for nonionic surfactants.<sup>36</sup> Time-resolved emission and fluorescence quenching studies of  $[\text{Ru}(\text{bpy})_3]^{2+}$  and several derivatives resulted in behavior that was nearly independent of  $\omega$  when probe and surfactant were of opposite charge but a significant dependence on  $\omega$  was seen when the probe and surfactant had the same charge.<sup>52,53</sup> Similarly, hydrophobic probes are often located in the interfacial region and exhibit shifts and dynamics that are independent of  $\omega$ .<sup>28,54</sup> A useful property of RMs is that they are nominally monodisperse. This allows the size of the water pool to be easily controlled by the value of  $\omega$ . The confinement effects depend on the size so that RMs can in principle be used to systematically vary the solvation characteristics and examine how the spectra and dynamics are affected.

Attempts to study confinement effects on the solvation properties of water are best achieved using optical probes that reside in the water core, so that the results pertain to the solvation environment without direct interfacial contact. Determination of probe location is important for analyzing the results of dynamics experiments, but it is often difficult. Faeder and Ladanyi have performed molecular dynamics simulations of  $\text{I}_2^-$  in an anionic RM that predict that the anionic solute prefers to reside in the center of the water pool formed by an anionic (AOT) surfactant.<sup>32</sup> This is not surprising considering that the probe and surfactant are both anionic and therefore experience Coulombic repulsion. In addition, small ions are generally very hydrophilic and would be expected to reside in the center of the water pool in the absence of Coulombic attraction between the probe and surfactant. However, in general, the location of a solute within a RM is difficult to unambiguously determine.

We have recently reported studies of FTIR spectra and ultrafast IR vibrational relaxation dynamics of azide,  $\text{N}_3^-$ , and other anions in nonionic NP (nonylphenol polyoxoethylene) RMs<sup>20,49,50</sup> as well as of azide in RMs made from anionic AOT (sodium bis(2-ethylhexyl) sulfosuccinate), cationic CTAB (cetyltrimethylammonium bromide), and the nonionic surfactant Brij-30.<sup>51</sup> We interpreted the results of both the dynamics and the static spectral shifts in terms of the location of azide within the RMs and its dependence on the surfactant charge. Azide resides in the most bulklike region in the center of the RM water pool for anionic AOT RMs, as evidenced by small spectral shifts from the bulk and dynamics that were indistinguishable from the bulk. For cationic CTAB, azide resides at or very near the interface, as evidenced by large static spectral shifts and relatively large decreases in VER rates that show little dependence on  $\omega$ . These results are most likely due to Coulombic interactions between the charged surfactant headgroups and the azide anion. In the nonionic RMs, the interface between the surfactant wall and the water pool is poorly defined due to the extended, hydrophilic poly-oxo groups of the surfactant. The water pool is not initially formed because the surfactant poly-oxo chains must be solvated before the water pools are formed. Therefore, azide resides within and interacts with the poly-oxo chains rather than a water pool for small RMs. The interaction depends on the length of the poly-oxo chains, with a stronger interaction for the longer chained NP surfactant due to a larger number of oxo groups. However, the segregation between the water and poly-oxo chains is greater in the RMs than in mixtures of  $\text{H}_2\text{O}$  and tri(ethylene glycol) monomethyl ether (TGE). TGE is a model of the hydrophilic portion of the nonionic surfactants that has a poly-oxo-chain without a hydrophobic end. This segregation allows for water pool

formation within the RM interior for large  $\omega$ , although the interface between the surfactant and water pool is not as well defined as with ionic surfactants.

In this study, we extend the VER studies in RMs to include a series of cyanoferrates that includes ferrocyanide  $[\text{Fe}(\text{CN})_6]^{4-}$ , ferricyanide  $[\text{Fe}(\text{CN})_6]^{3-}$ , and sodium nitroprusside  $[\text{SNP}, \text{Fe}(\text{CN})_5\text{NO}_2^-]$ . Following initial reports of vibrational and rotational dynamics of ferrocyanide in  $\text{D}_2\text{O}$  and  $\text{H}_2\text{O}$  using infrared transient gratings by Ohta et al.,<sup>55,56</sup> we recently studied the steady state and ultrafast infrared spectroscopy of the cyanoferrates in bulk solution.<sup>57</sup> The cyanoferrates are ions that are larger than the previously studied pseudohalide ions.<sup>20,49–51</sup> VER studies of bulk solution triatomic anions serve as a baseline set of results, and the studies of cyanoferrates and RMs can be viewed as exploring how spectral and dynamical properties are affected in more complex solutes or solvation environments, respectively. Cyanoferrates resemble metal hexacarbonyls, which are benchmark systems for studies of VER dynamics,<sup>58–62</sup> but the ionic nature of the former restricts their solubility to water and other highly polar solvents such as formamide. Their longer vibrational relaxation ( $T_1$ ) times enable a much more accurate determination of anisotropy decay times ( $T_r$ ) than is possible with azide. In addition, the cyanoferrates exhibit two different mechanisms for anisotropy decay. The anisotropy decays via normal molecular reorientation for the nondegenerate NO band of SNP, as well as via a dipolar reorientation mechanism for the hexacyanates where the transition dipole is exchanged between degenerate vibrations. In our bulk VER studies,<sup>57</sup> we found no simple correlations between the VER rate and other static spectral properties. The cyanoferrates exhibit much more complicated VER dynamics than azide, in which there is a strong correlation between the static spectral shift and the VER rate.<sup>50,63,64</sup> The complex vibrational properties may be in part due to additional intramolecular vibrational redistribution (IVR) pathways from the additional normal modes of the larger anions. These IVR pathways can be solvent assisted, leading to complex solvent–solute interactions with many possible relaxation pathways that do not lend themselves to a simple explanation. In addition, the CN band of SNP is very weak and has slow VER dynamics because of electronic effects. This points to different mechanisms that can control the spectral shift and VER rates in the cyanoferrates.

In the present study, we investigate larger anions with more complex relaxation dynamics to see whether the surfactant charge effects seen for azide in RMs also occur for larger solutes. Overall, the dependence on surfactant charge is similar in the cyanoferrates as in azide, but the differences in solute size and charge lead to different behavior in some instances. Again, the extent to which the vibrational properties are changed increases as the surfactant charge becomes more positive. The effects are largest for CTAB, smallest for AOT, and intermediate for the nonionic surfactants. Ferrocyanide, with a much higher negative charge, prefers a much more bulklike environment than does azide. SNP, which is less hydrophilic than azide, consistent with its high solubility in nonaqueous solvents, shows a large dependence on surfactant charge with much ( $\sim 7$  times) longer  $T_1$  times in cationic CTAB RMs. SNP also has a much more favorable interaction with the poly-oxo chains of the nonionic RMs, leading to an inhomogeneous distribution of sites within the RM interior that exhibit differing vibrational frequencies,  $T_1$  times, and in some cases,  $T_r$  times. As reported for azide,<sup>51</sup> we also measured SNP in TGE/water mixtures to help interpret the results in nonionic RMs.

## Experimental Section

Details of the laser system can be found in a previous publication.<sup>50</sup> Briefly, the laser system consists of a CW pumped (Nd:VO<sub>4</sub>, Spectra-Physics Millennia) titanium sapphire oscillator (Clark NJA-5) amplified in a regenerative amplifier pumped by a Nd:YLF (Positive Light Merlin) laser providing  $\sim 100$  fs pulses with an energy of  $\sim 900$   $\mu$ J at 1 kHz. The amplified output pumps an optical parametric amplifier (TOPAS, Light Conversion) generating 150  $\mu$ J of combined signal (1150–1600 nm) and idler (1600–2700 nm) radiation. Mid-IR pulses (2.4 to 11  $\mu$ m) are generated by difference frequency mixing of the TOPAS output pulses in a Type I AgGaS<sub>2</sub> crystal (2 mm) after traveling through a quartz time plate. This provides IR pulses of  $\sim 4$   $\mu$ J and 200 fs near 5  $\mu$ m that are split into two components. The probe component (10%) is directed to a translation stage and through the sample. The pump component is directed to a mechanical chopper operating at 500 Hz and crossed with the probe at a small angle at the sample after passing through a 75 mm focal length CaF<sub>2</sub> lens. The probe beam polarization is controlled via a wire grid polarizer after the sample. The probe beam is sent to a monochromator with  $\sim 5$   $\text{cm}^{-1}$  resolution and detected with an HgCdTe infrared detector (Santa Barbara Research Center, model 40742). The signal is processed with a pair of lock-in amplifiers (Stanford Research Systems SR 530) and gated integrators (Stanford Research Systems SR 250) to determine the pump-induced absorbance change. FTIR spectra were taken with a Mattson 7020A spectrometer using 25 scans with 1  $\text{cm}^{-1}$  resolution.

AOT, NP, and Brij-30 samples, as described previously,<sup>49–51</sup> were prepared by adding the appropriate amount of an aqueous solution containing the cyanoferrate probe molecule to a nominally  $\omega = 0$  solution of the corresponding surfactant solution. The NP surfactants used were NP7 (IGEPAL CO-610) and NP4 (IGEPAL CO-430) in a 4:1 volume ratio. NP concentrations refer to the NP7 concentration and  $\omega = [\text{H}_2\text{O}]/[\text{NP}]$ . The solutions were then sonicated until a clear solution resulted. CTAB is not soluble in anhydrous CH<sub>2</sub>Cl<sub>2</sub>, so the appropriate amounts of CTAB, CH<sub>2</sub>Cl<sub>2</sub>, and aqueous probe solution were combined and shaken until a clear solution resulted. Surfactant concentrations were 0.2 M AOT in *n*-heptane, 0.3 M NP in cyclohexane, 0.3 M Brij-30 in cyclohexane, and 0.1 or 0.3 M CTAB in CH<sub>2</sub>Cl<sub>2</sub>. In general, a constant aqueous solute concentration of probe was used for all values of  $\omega$ , resulting in larger sample absorbances for larger  $\omega$  RMs. Sample path lengths were 250 or 500  $\mu$ m for RM solutions and 50  $\mu$ m for H<sub>2</sub>O/TGE mixtures using a static cell (Harrick) with CaF<sub>2</sub> windows and variable path length Teflon spacers. H<sub>2</sub>O was obtained from a Milli-Q purification system. All other solvents and solutes were purchased from Aldrich and used as received. All experiments were performed at ambient room temperature.

## Results

**FTIR.** There were a limited number of RMs and  $\omega$  values, AOT ( $\omega = 4$  to 14) and Brij-30 ( $\omega = 1$ –3), for which ferrocyanide was stabilized. Figure 1 shows FTIR spectra of ferrocyanide as a function of  $\omega$  in RMs made with 0.2 M AOT/*n*-heptane and 0.3 M Brij-30/cyclohexane, along with the bulk H<sub>2</sub>O spectrum. The bottom of Figure 1 shows the peak position as a function of  $\omega$ . A small blue shift of  $\sim 3.5$   $\text{cm}^{-1}$  is seen for the smallest RM,  $\omega = 1$  Brij-30, and the peak shifts toward the bulk as  $\omega$  is increased. Figure 2 shows the IR band peak positions of ferricyanide as a function of  $\omega$  for all four RM systems studied. The largest red shift is seen for the cationic

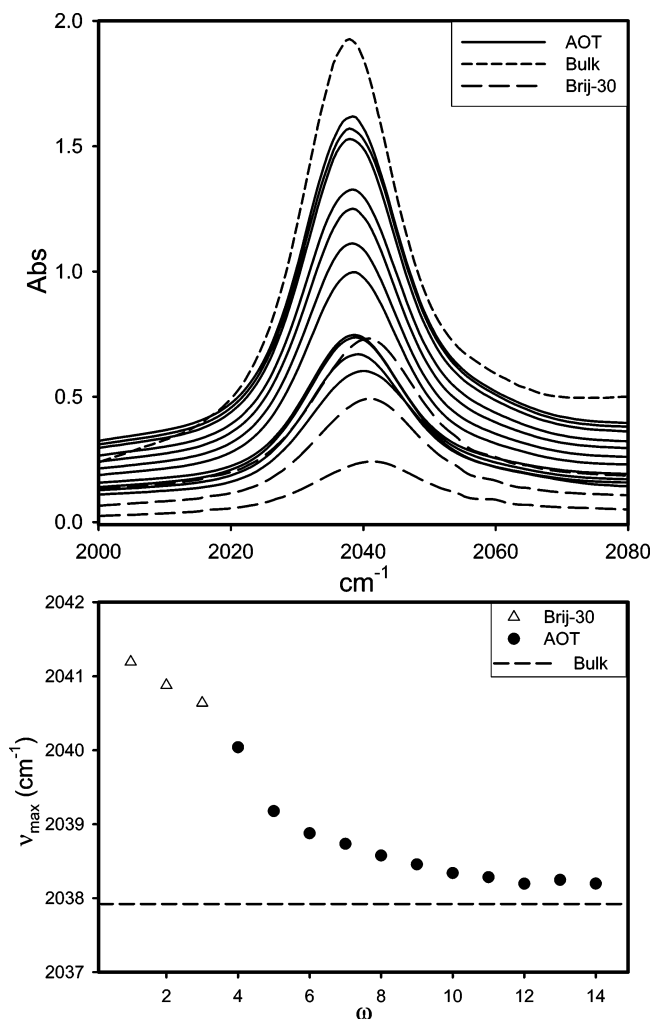


**Figure 1.** (Top) FTIR spectra of ferrocyanide in 0.2 M AOT/*n*-heptane ( $\omega = 4$ –14) and 0.3 M Brij-30/cyclohexane ( $\omega = 1$ –3) RMs as a function of  $\omega$ . Concentrations of ferrocyanide in the aqueous solution are 0.14 M for Brij-30 RMs and 0.11 M for AOT RMs, with 250 and 500  $\mu$ m spacers, respectively. Spectra are obtained by subtracting the  $\omega = 0$  spectra and offset due to increasing H<sub>2</sub>O absorption with increasing  $\omega$ . (Bottom) corresponding FTIR spectral peaks as a function of  $\omega$ .

surfactant CTAB; it is  $\sim 5$   $\text{cm}^{-1}$  at  $\omega = 3$ , decreases to  $\sim 4$   $\text{cm}^{-1}$  for  $\omega = 5$ , and remains nearly constant up to  $\omega = 8$ , above which the RMs with azide are not stable. NP has the second largest red shift,  $\sim 4$   $\text{cm}^{-1}$  at  $\omega = 1$ , and steadily approaches the bulk value as  $\omega$  increases, decreasing to 2.5  $\text{cm}^{-1}$  at  $\omega = 11$ . In Brij-30 the IR band is red shifted by 3  $\text{cm}^{-1}$  at  $\omega = 1$  and steadily approaches the bulk as  $\omega$  increases, with a  $\sim 0.5$   $\text{cm}^{-1}$  red shift for  $\omega > 11$ . For ferricyanide in AOT RMs, the peak of the IR band is not shifted at all from the bulk value in the range  $\omega = 4$  to  $\omega = 14$ , the entire range of RM stability. Another interesting feature was the apparent formation of ferrocyanide in the ferricyanide/AOT RMs. Besides the band in the region expected for ferricyanide,  $\sim 2115$   $\text{cm}^{-1}$ , a second IR band appeared near 2040  $\text{cm}^{-1}$ . This second band had the same peak position as a function of  $\omega$  as the ferrocyanide band in AOT. We assume that a partial reduction of ferricyanide to ferrocyanide occurs in AOT RMs. Although the separation between the vibrational bands was large enough to pump only the ferricyanide band, we chose not to perform dynamics studies of ferricyanide in AOT because of the uncertainty about the long-term stability of the solutions as well as the small sample absorbance, which would result in small transient signals.



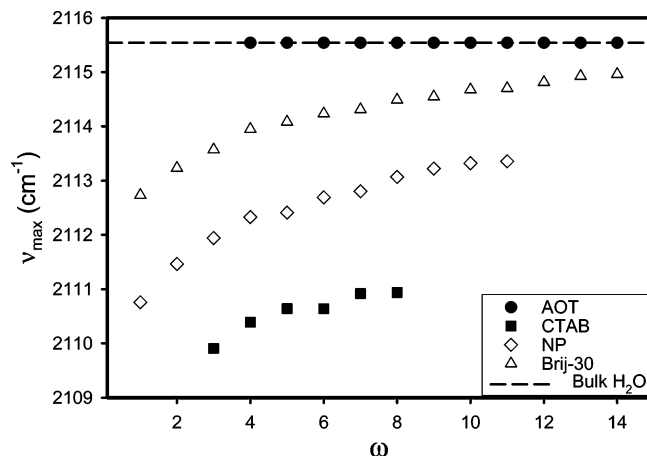


**Figure 2.** Vibrational band centers from FTIR spectra for ferricyanide in 0.3 M Brij-30/cyclohexane, 0.3 M NP/cyclohexane, 0.2 M AOT/*n*-heptane, and 0.3 M CTAB/ $\text{CH}_2\text{Cl}_2$  RMs as a function of  $\omega$ . Concentrations of ferricyanide in the aqueous phase are 0.1 M for AOT RMs, 0.2 M for NP and Brij-30 RMs, and 0.3 M for CTAB RMs.

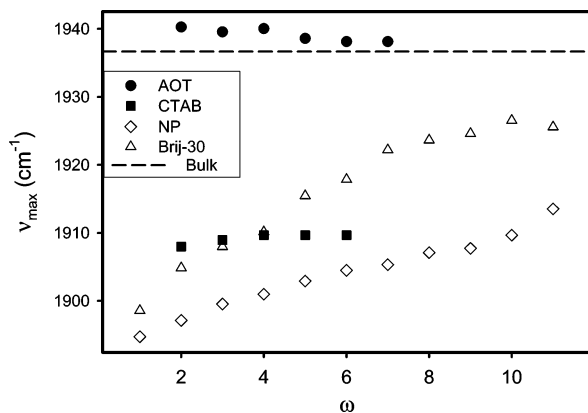


**Figure 3.** Vibrational band centers from FTIR spectra for the NO band of SNP in 0.2 M AOT/*n*-heptane, 0.3 M Brij-30/cyclohexane, 0.3 M NP/cyclohexane, and 0.1 M CTAB/ $\text{CH}_2\text{Cl}_2$  RMs as a function of  $\omega$ . Concentrations of SNP in aqueous solution are 0.22 M for AOT RMs, 0.85 M for Brij-30 and NP RMs, and 0.5 M for CTAB RMs.

Figure 3 shows the peak position of the NO band of SNP in all four RM systems. In AOT, a small blue shift of  $3.5 \text{ cm}^{-1}$  at  $\omega = 2$  decreases as  $\omega$  increases to  $1.5 \text{ cm}^{-1}$  at  $\omega = 7$ . For CTAB RMs, a large red shift of  $29 \text{ cm}^{-1}$  is seen for  $\omega = 2$  that is only reduced by  $2 \text{ cm}^{-1}$  at  $\omega = 4$  and remains constant up to  $\omega = 6$ , the largest stable micelle. For the nonionic RMs, Brij-30 and NP, a large red shift is seen for small RMs that steadily approaches the bulk value as the RM size is increased. However, the shape of the IR band in the nonionic RMs is not so simple and merits closer scrutiny. Figure 4 shows the SNP IR spectra in NP and Brij-30 RMs at several values of  $\omega$  along with the bulk  $\text{H}_2\text{O}$  spectrum. Unlike AOT and CTAB where the bandwidth in the RMs is similar to that in the bulk, the band is much broader in the nonionic RMs, especially at high  $\omega$ . In addition, the band is asymmetric and is double peaked at high  $\omega$  for Brij-30 RMs. The band shape did not show any change upon a 10-fold reduction in SNP concentration. For comparison purposes, Figure 4 also shows FTIR spectra of the NO band of SNP in bulk TGE as well as in  $\text{H}_2\text{O}/\text{TGE}$  mixtures corresponding to the  $\omega$  values of the RMs, where  $\omega$  corresponds to the molar ratio of  $\text{H}_2\text{O}$  to TGE. For the  $\text{H}_2\text{O}/\text{TGE}$  mixtures, the IR band peak positions are intermediate between the NP and Brij-30 RM peak positions and are symmetric in all cases. In addition, the bands have a fairly constant bandwidth that is

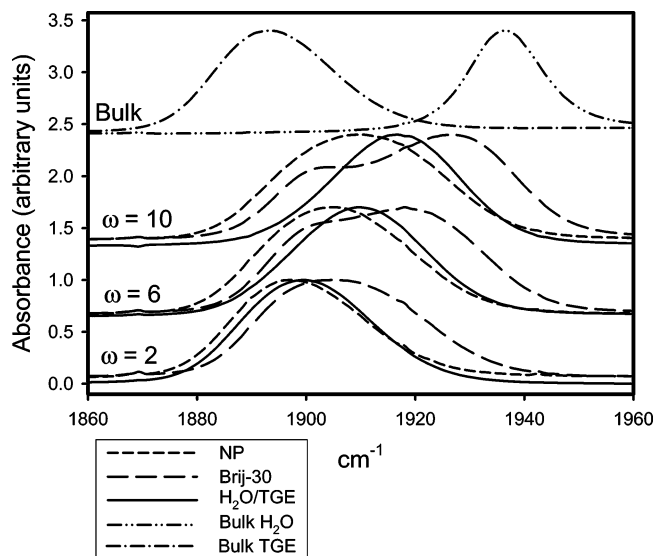


**Figure 4.** FTIR spectra of the NO band of SNP in Brij-30 RMs (long dash), NP RMs (short dash), and  $\text{H}_2\text{O}/\text{TGE}$  mixtures (solid) for  $\omega = 2, 6$ , and  $10$ . Also included are bulk  $\text{H}_2\text{O}$  (dash-dot-dot) and bulk TGE (dash-dot). RM spectra are obtained by subtracting the  $\omega = 0$  spectra, and those in bulk solution are solvent subtracted. All spectra are normalized.

similar to bulk TGE and narrower than in the nonionic RMs, especially at high  $\omega$ .

**Vibrational and Rotational Dynamics.** Some representative transient decays and their respective fits are shown in Figure 5. Included are both the population dynamics taken with pump and probe beam polarizations oriented at the magic angle and the decay in the anisotropy. The anisotropy,  $r(t)$ , for both transient absorptions and transient bleaches is defined as

$$r(t) = \frac{I_{\parallel}(t) - I_{\perp}(t)}{I_{\parallel}(t) + 2I_{\perp}(t)}$$

where  $I_{\parallel}(t)$  and  $I_{\perp}(t)$  are the transient signal measured with the relative pump and probe beam polarizations parallel and perpendicular, respectively. Figure 6 shows  $T_1$  and  $T_r$  times for ferrocyanide in AOT and Brij-30 RMs as a function of  $\omega$  along with the values for bulk  $\text{H}_2\text{O}$ . In all cases the  $T_1$  and  $T_r$  times in the RMs are very similar to, and often within the uncertainty of, the bulk  $\text{H}_2\text{O}$  values of  $4.4 \pm 0.5 \text{ ps}$  for  $T_1$  and  $2.1 \pm 0.5 \text{ ps}$  for  $T_r$ .<sup>57</sup> There is no obvious trend for either  $T_1$  or  $T_r$  with  $\omega$ . Figure 7 shows  $T_1$  and  $T_r$  times for ferricyanide in CTAB, NP, and Brij-30 RMs as a function of  $\omega$  along with the values for bulk  $\text{H}_2\text{O}$ . No data were taken for AOT due to apparent formation of ferrocyanide in AOT RMs. For NP and Brij-30 RMs,  $T_1$  and  $T_r$  times in the RMs are within the uncertainty of the bulk  $\text{H}_2\text{O}$  values of  $7 \pm 1 \text{ ps}$  for  $T_1$  and  $3.3 \pm 0.5 \text{ ps}$  for  $T_r$ .<sup>57</sup> For CTAB RMs,  $T_r$  is within the uncertainty of the bulk value, but  $T_1$  at  $\omega = 5$ ,  $9.7 \pm 1 \text{ ps}$ , is slightly longer than seen in the bulk.  $T_1$  and  $T_r$  times for ferricyanide and ferrocyanide in RMs are summarized in Table 1.

$T_1$  and  $T_r$  times for the NO band of SNP in AOT and CTAB RMs as a function of  $\omega$ , along with bulk values,<sup>57</sup> are shown in Figure 8 and are listed in Table 1. In AOT,  $T_1$  times are within the uncertainty of the bulk, however,  $T_r$  times are 2–3 times longer. For CTAB RMs,  $T_1$  and  $T_r$  times are much longer (6–7 times) than seen in bulk  $\text{H}_2\text{O}$ . A clear trend of decreasing  $T_1$  for larger  $\omega$  is seen for CTAB RMs.  $T_r$  may be increasing with  $\omega$ , but the large uncertainties obscure any real trend.  $T_1$  and  $T_r$  times for SNP in the nonionic RMs Brij-30 and NP depend on

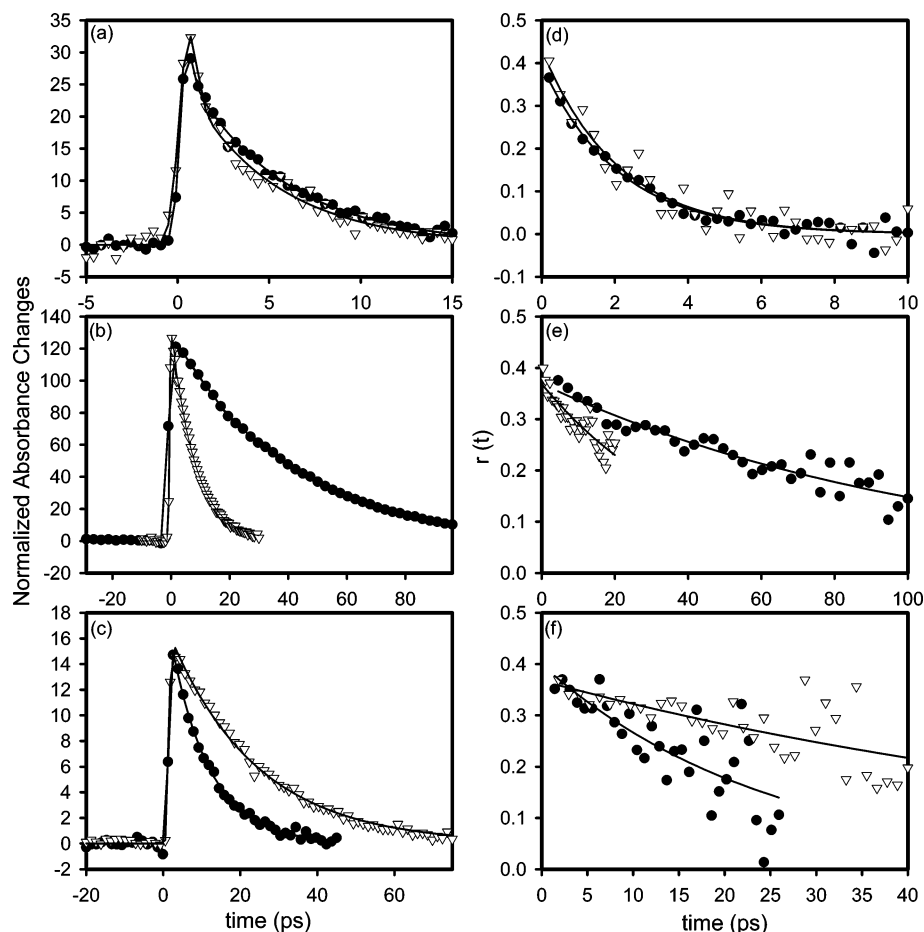


**Figure 5.** Representative transients of population decay for (a) ferrocyanide in  $\omega = 8$  AOT at  $2045\text{ cm}^{-1}$  (circles) and  $\omega = 1$  Brij-30 RMs at  $2040\text{ cm}^{-1}$  (open triangles), (b) SNP in  $\omega = 6$  CTAB at  $1905\text{ cm}^{-1}$  (circles) and  $\omega = 6$  AOT RMs at  $1940\text{ cm}^{-1}$  (open triangles), and (c) SNP in  $\omega = 10$  NP RMs at  $1935\text{ cm}^{-1}$  (circles) and  $1905\text{ cm}^{-1}$  (open triangles). Representative transients of anisotropy decay for (d) ferrocyanide in  $\omega = 8$  AOT at  $2045\text{ cm}^{-1}$  (circles) and  $\omega = 2$  Brij-30 RMs at  $2040\text{ cm}^{-1}$  (open triangles), (e) SNP in  $\omega = 6$  CTAB at  $1908\text{ cm}^{-1}$  (circles) and  $\omega = 6$  AOT RMs at  $1940\text{ cm}^{-1}$  (open triangles), and (f) SNP in  $\omega = 10$  Brij-30 RMs at  $1935\text{ cm}^{-1}$  (circles) and  $1915\text{ cm}^{-1}$  (open triangles). All transients correspond to bleaches of the static ground-state absorption. The points are the data and the lines are calculated from constants determined from fitting. The decay constants determined can be found in Tables 1–3.

detection/probe IR frequency. This dependence can be seen in Figure 5c and 5f, where the transients differ only in probe frequency chosen by the monochromator. It must be noted that broadband IR excitation is used, preventing determination of the rates of spectral diffusion, if any, on our time scale, of the apparently inhomogeneous IR absorption. The transient decays were fit to a single exponential and including additional exponential terms did not improve the fit. The  $T_1$  and  $T_r$  times as a function of frequency along with the static IR absorption spectra are given in Figure 9 and Figure 10 for Brij-30 and NP RMs, respectively, for  $\omega = 2, 6$ , and  $10$ . These data are also summarized in Table 2. The data include both transient bleaches (higher frequency data) and transient absorptions (lower frequency data). In general, the  $T_1$  time is shorter on the blue side of the absorption band for both nonionic RM systems. Overall,  $T_1$  times are shorter for Brij-30 than NP and  $T_1$  times are shorter for larger  $\omega$ .  $T_r$  times for Brij-30 RMs are shorter on the blue side of the absorption band and are shorter for larger  $\omega$ . The  $T_r$  times for NP RMs show little dependence on frequency or  $\omega$ . They are  $>100\text{ ps}$  in all cases and are therefore hard to precisely determine due to the much shorter  $T_1$  times. Figure 11 shows the  $T_1$  times, along with the static IR absorption spectra, of SNP in  $\text{H}_2\text{O}/\text{TGE}$  mixtures for  $\omega = 2, 6$ , and  $10$  and for bulk TGE. The  $T_1$  and  $T_r$  times are summarized in Table 3. A frequency dependence is also seen for  $T_1$  times in the  $\text{H}_2\text{O}/\text{TGE}$  mixtures, but it is much smaller than in the nonionic RMs and similar to

that seen for bulk TGE.  $T_1$  times are again shorter on the blue side of the static absorption band and are also shorter for larger values of  $\omega$ . It was observed that the  $T_1$  time decreased significantly on the very red edge of the transient absorption, reaching a value similar to what was measured on the blue edge of the transient bleach. Similar behavior was seen in the RMs, but  $T_1$  times on the red edge of the transient absorption remained significantly longer than on the blue edge of the bleach. The  $T_r$  times for  $\text{H}_2\text{O}/\text{TGE}$  mixtures were measured for relatively high-frequency probes and were too long ( $>100\text{ ps}$ ) to measure in all cases.

## Discussion

**Bulk Cyanoferrates.** The vibrational and rotational dynamics of the cyanoferrates in bulk solution have been previously reported.<sup>55–57</sup> Unlike the small azide ion,<sup>50,51,63–65</sup> there were no clear correlations between the vibrational frequencies and the VER rates as a function of solvent. Overall, we were unable to identify a simple explanation for the VER times based simply on charges, vibrational frequencies, or IR absorption intensities that is consistent across the entire data series. However, a general trend was seen in the VER rates that followed the polarity/H-bonding characteristics of the solvent, with rates in the following order:  $\text{H}_2\text{O} > \text{D}_2\text{O} > \text{MeOH} \sim \text{formamide} \sim \text{ethylene glycol} > \text{DMSO}$ . The VER rate of the CN band of SNP

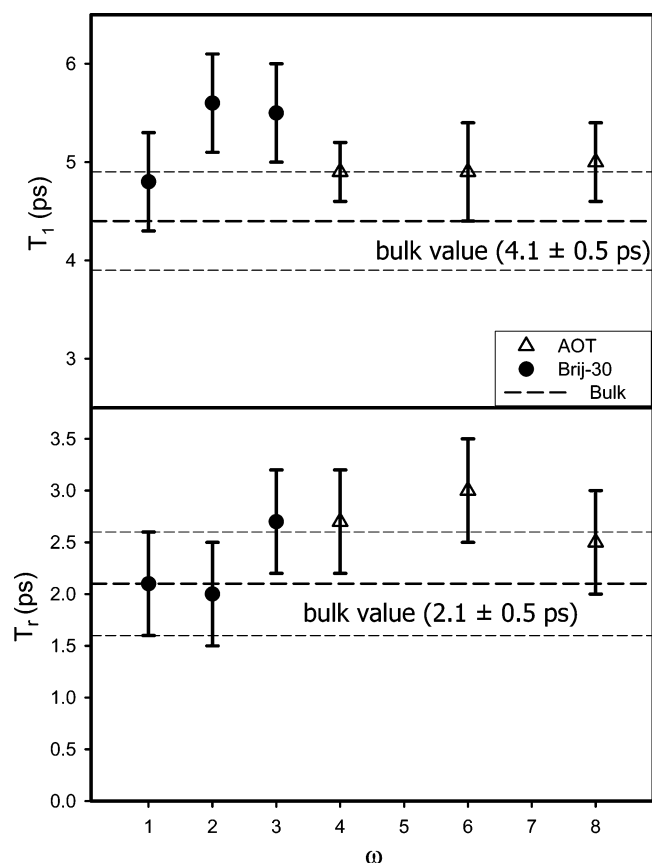


**Figure 6.**  $T_1$  and  $T_r$  for ferrocyanide in AOT (open triangle) and Brij-30 (circles) RMs as a function of  $\omega$ . The dashed line indicates the bulk  $H_2O$  value from ref 57.

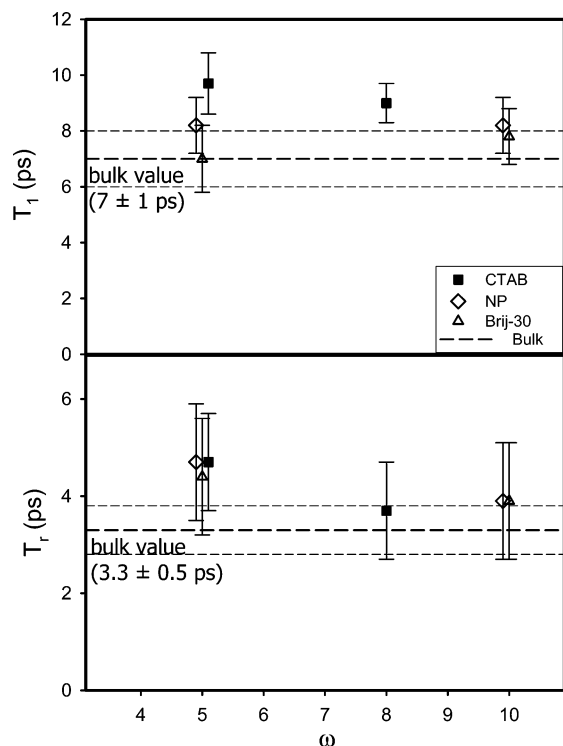


**Figure 7.**  $T_1$  and  $T_r$  for ferricyanide in CTAB (squares), NP (open diamonds), and Brij-30 (open triangles) RMs as a function of  $\omega$ . The dashed line indicates the bulk  $H_2O$  value from ref 57.

was much slower than the NO band of SNP or the CN bands of ferrocyanide and ferricyanide. In addition, the transient signals of the CN band of SNP were very small due to the small

**TABLE 1:**  $T_1$  and  $T_r$  Times Measured for Cyanoferrates in Reverse Micelles

Ferrocyanide					
$\omega$	AOT		Brij-30		
	$T_1$ (ps)	$T_r$ (ps)	$T_1$ (ps)	$T_r$ (ps)	
1			$4.8 \pm 0.3$	$2.1 \pm 0.5$	
2			$5.6 \pm 0.5$	$2.0 \pm 0.5$	
3			$5.5 \pm 0.5$	$2.7 \pm 0.5$	
4	$4.9 \pm 0.3$	$2.7 \pm 0.5$			
6	$4.9 \pm 0.5$	$3.0 \pm 0.5$			
8	$5.0 \pm 0.4$	$2.5 \pm 0.5$			
bulk $H_2O^a$	$4.4 \pm 0.5$	$2.1 \pm 0.5$			
Ferricyanide					
$\omega$	NP		Brij-30		
	$T_1$ (ps)	$T_r$ (ps)	$T_1$ (ps)	$T_r$ (ps)	
5	$8.2 \pm 1$	$4.7 \pm 1.2$	$7.0 \pm 1.2$	$4.4 \pm 1.2$	$9.7 \pm 1.1$
8					$9.0 \pm 0.7$
10	$8.2 \pm 1$	$3.9 \pm 1.2$	$7.8 \pm 1.0$	$3.9 \pm 1.2$	$3.7 \pm 1.0$
bulk $H_2O^a$	$7.0 \pm 1$	$3.3 \pm 0.5$			
SNP					
$\omega$	AOT		CTAB		
	$T_1$ (ps)	$T_r$ (ps)	$T_1$ (ps)	$T_r$ (ps)	
2			$53 \pm 5$	$90 \pm 30$	
4			$45 \pm 4$	$105 \pm 30$	
6	$8.0 \pm 0.6$	$44 \pm 5$	$41 \pm 4$	$120 \pm 25$	
7	$8.1 \pm 0.8$	$46 \pm 5$			
bulk $H_2O^a$	$7.3 \pm 0.8$	$16 \pm 5$			

<sup>a</sup> Data from ref 57.

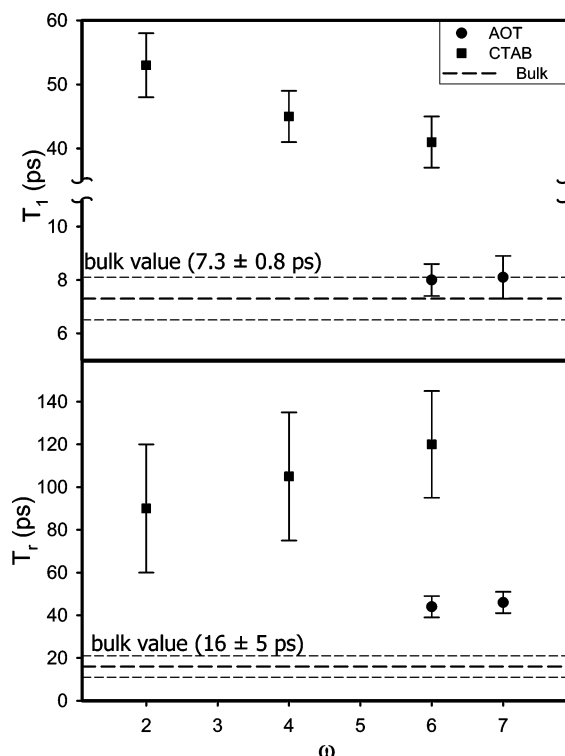


**Figure 8.**  $T_1$  and  $T_r$  for the NO band of SNP in anionic AOT (circles) and cationic CTAB (squares) RMs as a function of  $\omega$ . The dashed line indicates the bulk  $H_2O$  value from ref 57.

transition dipole moment. For this reason we did not perform extensive experiments on this band in RMs. Ferricyanide exhibited the smallest VER rate dependence on solvent, ferrocyanide had the largest solvent dependence, and SNP was intermediate. In addition, only the NO band of SNP showed a large peak frequency dependence on solvent, primarily due to

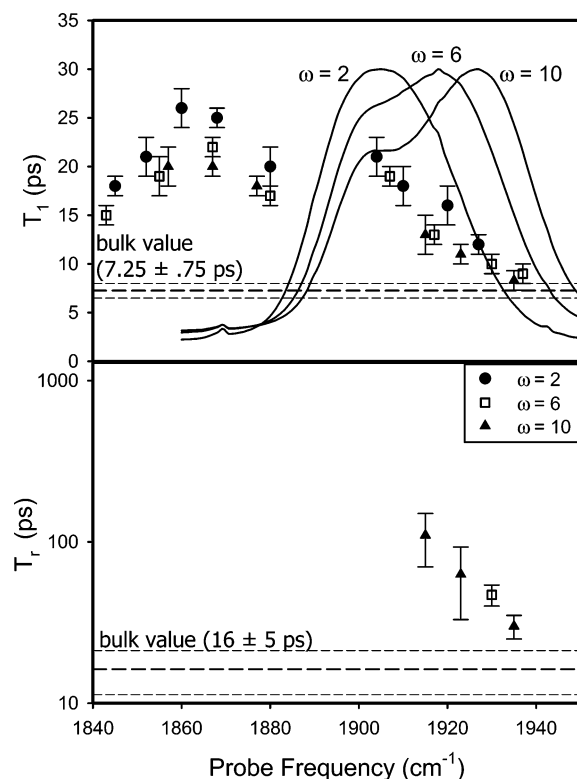


**Figure 9.**  $T_1$  and selected  $T_r$  times for the NO band of SNP in Brij-30 RMs for  $\omega = 2, 6$ , and  $10$ . The static IR spectra are included. RM spectra are obtained by subtracting the  $\omega = 0$  spectra and normalizing to a constant maximum. Data obtained with concentrations of SNP in the aqueous phase ranging from  $0.28$  to  $0.85$  M showed no significant concentration dependence.  $T_r$  times are shown only for samples where  $T_r$  was short enough to be well defined.

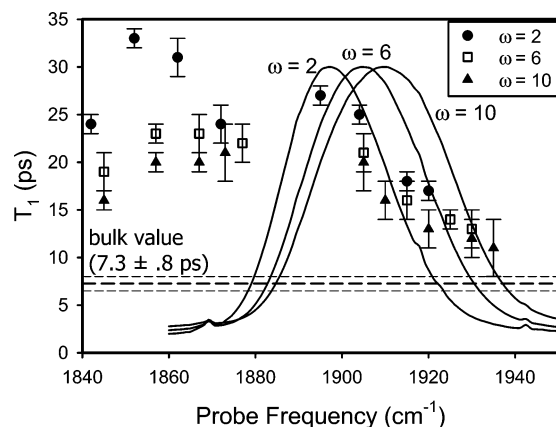


**Figure 10.**  $T_1$  times for the NO band of SNP in NP RMs for  $\omega = 2, 6$ , and  $10$ . The static IR spectra are included. RM spectra are obtained by subtracting the  $\omega = 0$  spectra and normalized to a constant maximum. Data obtained with concentration of SNP in aqueous phase ranging from  $0.28$  to  $0.85$  M showed no significant concentration dependence.

interactions between the solvent and the CN groups.<sup>66</sup> The electron withdrawing nature of NO may be responsible for both the small band intensity and long  $T_1$  time of the CN band of SNP.<sup>57</sup> In addition, the solubility characteristics of the charged cyanoferrates and the neutral metal carbonyls appear to be an important factor in determining the VER rates. The charged species are soluble in more strongly interacting polar solvents resulting in faster VER rates.<sup>57</sup>

**Ferrocyanide.** Upon RM formation, the IR absorption of the CN stretch of ferrocyanide undergoes only a slight blue shift

from the bulk H<sub>2</sub>O value. For the smallest RM the shift is  $\sim 3.5$  cm<sup>-1</sup> and approaches the bulk value as  $\omega$  increases. In bulk solvents, the largest shift from bulk water was a  $2$  cm<sup>-1</sup> red shift in formamide. This is similar to what was observed for azide in AOT, where the blue shift was attributed to increased ionic strength from the Na<sup>+</sup> counterions of AOT.<sup>20</sup> However, saturating an aqueous solution of ferrocyanide with NaCl induces of blue shift in the CN stretch of only  $\sim 1$  cm<sup>-1</sup>. In addition, the largest blue shift is seen for the nonionic RM Brij-30, where the concentration of ferrocyanide was kept constant in the aqueous phase, ruling out ionic strength effects as the origin of the blue shift. The bulk solvent studies suggest a red shift when the polarity is decreased. Because the polarity is expected to decrease in a RM, the origin of the blue shift is not completely clear. The blue shift could be due to increased association with the K<sup>+</sup> counterions in the RMs, but the change in dissociation constants upon confinement is unknown. In addition, if counterion association were the source of the blue shift, a larger blue shift would be expected in AOT RMs due to the presence of additional Na<sup>+</sup> counterions for the AOT surfactant.

For ferrocyanide in AOT RMs, both the  $T_1$  and  $T_r$  times are indistinguishable from the bulk H<sub>2</sub>O values. This suggests that ferrocyanide is located in the most bulklike region of the RM interior in the center of the water pool. This is also supported by the fact that the red shift of the static spectrum in bulk solution is not observed in the RMs, and that the  $T_1$  time exhibits a large bulk solvent dependence. In bulk solvents the  $T_1$  time is much shorter in H<sub>2</sub>O than other solvents, including D<sub>2</sub>O, formamide, and ethylene glycol, where  $T_1$  is increased by a factor of  $5$  to  $10$ .<sup>57</sup> If the solvation environment in the RMs were significantly different than in bulk H<sub>2</sub>O we would expect to see a significant change in the  $T_1$  time. Simulations<sup>31</sup> and experiments<sup>13,67</sup> suggest that the bound layer extends  $4$ – $5$  Å from the surfactant headgroups. Bulklike free water fills in the remaining portion of the RM interior. The radius of the AOT RMs studied range from  $\sim 15$  Å ( $\omega = 4$ ) to  $\sim 20$  Å ( $\omega = 8$ ), with  $\sim 140$  to  $\sim 600$  water molecules per RM.<sup>31,68</sup> The resulting pools of free water are apparently large enough (radii  $\geq 10$  Å) to provide a bulklike environment for the ferrocyanide ion, with a radius of  $\sim 3.5$  Å. The similarity of the  $T_r$  time in bulk H<sub>2</sub>O and AOT RMs is not surprising due to the mechanism of the anisotropy decay process, which involves an exchange between degenerate modes and more closely resembles VER than rotational dynamics.<sup>57</sup> Also, in bulk solvents the  $T_r$  time showed a much smaller solvent dependence than the  $T_1$  times, so the  $T_r$  times are apparently not very sensitive to the location of ferrocyanide in AOT RMs; i.e., dipolar reorientation is less sensitive than rotational reorientation.

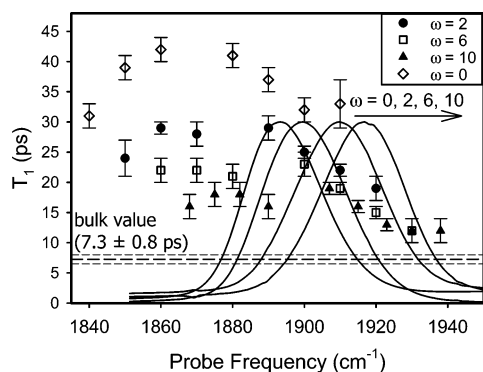
For Brij-30 RMs, the  $T_1$  and  $T_r$  times of ferrocyanide, as indicated in Figure 6, are again similar to the values in bulk H<sub>2</sub>O. This suggests that ferrocyanide also resides in a bulklike region in the center of the water pool of these RMs. However, solvation of the poly-oxo chains of Brij-30 generally prevents water pool formation for the small values of  $\omega$  used here.<sup>28,29,33,69–71</sup> For azide in Brij-30, the  $T_1$  time was significantly longer for small  $\omega$  RMs and steadily approached the bulk value as  $\omega$  increased. This was attributed to the interaction of azide with the poly-oxo chains leading to a changing solvation environment until  $\omega$  was large enough for water pools to completely form. The ferrocyanide data are not consistent with this type of behavior. Due to the larger negative charge and increased hydrophilic nature of ferrocyanide, water may preferentially solvate ferrocyanide rather than the poly-oxo chains,

TABLE 2:  $T_1$  and  $T_r$  Times Measured for SNP in Nonionic Reverse Micelles

Brij-30								
$\omega = 2$			$\omega = 6$			$\omega = 10$		
$\nu_{\text{probe}} (\text{cm}^{-1})$	$T_1$ (ps)	$T_r$ (ps)	$\nu_{\text{probe}} (\text{cm}^{-1})$	$T_1$ (ps)	$T_r$ (ps)	$\nu_{\text{probe}} (\text{cm}^{-1})$	$T_1$ (ps)	$T_r$ (ps)
1845	$18 \pm 1$		1843	$15 \pm 1$		1857	$20 \pm 2$	$>150$
1852	$21 \pm 2$		1855	$19 \pm 2$	$>200$	1867	$20 \pm 1$	$>200$
1860	$26 \pm 2$		1867	$22 \pm 1$	$>350$	1877	$18 \pm 1$	$>200$
1868	$25 \pm 1$	$>400$	1880	$17 \pm 1$	$>200$	1915	$13 \pm 2$	$110 \pm 40$
1880	$20 \pm 2$	$>400$	1907	$19 \pm 1$	$>280$	1923	$11 \pm 1$	$63 \pm 29$
1904	$21 \pm 2$	$>400$	1917	$13 \pm 1$	$>220$	1935	$8.3 \pm 1$	$30 \pm 5$
1910	$18 \pm 2$		1930	$10 \pm 1$	$47 \pm 7$			
1920	$16 \pm 2$	$>400$	1937	$9 \pm 1$				
1927	$12 \pm 1$							
bulk $\text{H}_2\text{O}^a$	$7.3 \pm 0.8$	$16 \pm 5$						

NP								
$\omega = 2$			$\omega = 6$			$\omega = 10$		
$\nu_{\text{probe}} (\text{cm}^{-1})$	$T_1$ (ps)	$T_r$ (ps)	$\nu_{\text{probe}} (\text{cm}^{-1})$	$T_1$ (ps)	$T_r$ (ps)	$\nu_{\text{probe}} (\text{cm}^{-1})$	$T_1$ (ps)	$T_r$ (ps)
1842	$24 \pm 1$		1845	$19 \pm 2$		1845	$16 \pm 1$	
1852	$33 \pm 1$		1857	$23 \pm 1$	$>150$	1857	$20 \pm 1$	$>300$
1862	$31 \pm 2$		1867	$23 \pm 2$		1867	$20 \pm 1$	$>200$
1872	$24 \pm 2$	$>400$	1877	$22 \pm 2$	$>300$	1873	$21 \pm 3$	$>400$
1887	$37 \pm 1$	$>400$	1905	$21 \pm 2$	$>400$	1905	$20 \pm 3$	$>300$
1895	$27 \pm 1$		1915	$16 \pm 2$		1910	$16 \pm 2$	$>300$
1904	$25 \pm 1$	$>400$	1925	$14 \pm 1$	$>300$	1920	$13 \pm 2$	$>400$
1915	$18 \pm 1$	$>400$	1930	$13 \pm 2$		1930	$12 \pm 2$	$>200$
1925	$17 \pm 1$					1935	$11 \pm 3$	
bulk $\text{H}_2\text{O}^a$	$7.3 \pm 0.8$	$16 \pm 5$						

<sup>a</sup> Data from ref 57.

**Figure 11.**  $T_1$  times for the NO band of SNP in bulk TGE ( $\omega = 0$ ) and  $\text{H}_2\text{O}/\text{TGE}$  mixtures for  $\omega = 2, 6$ , and  $10$ . The static IR spectra are included.  $\text{H}_2\text{O}/\text{TGE}$  mixture spectra are obtained by subtracting the corresponding solvent spectrum and normalized to a constant maximum.

and the interaction between ferrocyanide and poly-oxo chains is unfavorable. These factors may mean that ferrocyanide has a stronger preference for regions where the local structure is dominated by water molecules than azide.<sup>51</sup> This may result in an inhomogeneous local structure, which may be expected from the nature of the nonionic micelles and the poorly defined interface. This is supported by the fact that azide is soluble in MeOH and bulk TGE, whereas ferrocyanide is not. For  $\text{H}_2\text{O}/\text{TGE}$  mixtures, ferrocyanide is not soluble unless the molar ratio of  $\text{H}_2\text{O}$  to TGE is high ( $\sim 20:1$  or greater). The very hydrophilic nature of ferrocyanide may also explain the instability of ferrocyanide containing NP RMs, where the longer poly-oxo chains of NP result in less free water and therefore may prevent the segregation necessary to allow solvation of ferrocyanide.

An apparent contradiction exists between the lack of a water pool and the bulklike VER dynamics of ferrocyanide in small  $\omega$  Brij-30 RMs. This contradiction sets up two possibilities. Ferrocyanide either affects the structure of the water within the RM or resides only in the highest polarity regions of water. To

distinguish between these possibilities, we added measurable quantities of the previously studied triatomic anions, cyanate ( $\text{NCO}^-$ )<sup>72</sup> and azide,<sup>51</sup> to ferrocyanide containing Brij-30 RMs and compared the spectra to those without ferrocyanide. The IR bands of azide and ferrocyanide overlap, making the analysis more difficult, but the data are not consistent with an increase in the amount of bulklike water. The  $\text{NCO}^-$  vibrational frequency exhibits small but measurable changes for water in the range of  $\omega$  studied, which complicates using it to detect any small perturbations. There were no measurable effects on the vibrational bands of  $\text{NCO}^-$  due to the addition of ferrocyanide, which provides evidence that adding ferrocyanide does not result in major changes in the RM structure. There is, however, an effect of reducing the range of  $\omega$  for Brij-30 RMs to  $\omega \leq 3$  due to adding enough ferrocyanide for IR studies, which is surprising because increasing the amount of water would be expected to enhance the solubility of ferrocyanide. The other possibility is that ferrocyanide is located in the bulklike core region of the water pool. If there were strong interactions with the surfactant headgroups we would expect slower VER dynamics. This is what is observed for CTAB RMs containing anionic probes; the VER times are longer than in bulk water by a factor of at least 2 and 7 for azide<sup>51</sup> and SNP, respectively.

**Ferricyanide.** The  $T_1$  and  $T_r$  times for ferricyanide in NP and Brij-30 RMs are within the uncertainty of the bulk values. At first glance, this suggests a bulklike environment for ferricyanide in the nonionic RMs. However, the uncertainties are large due to the relatively small signals, and the  $T_1$  times are not very sensitive to solvent in bulk solution.<sup>57</sup> These factors lead to ambiguity in this conclusion. The  $T_1$  times for ferricyanide in CTAB RMs are longer than the bulk  $T_1$  time, even when considering the large uncertainties. This could be indicative of an interaction between the ferricyanide anion and the cationic headgroups of CTAB, similar to what is seen for azide.<sup>51</sup> However, the small number of samples that can be investigated



**TABLE 3:  $T_1$  and  $T_r$  Times Measured for SNP in Bulk TGE and H<sub>2</sub>O/TGE Mixtures**

TGE			$\omega = 2$			$\omega = 6$			$\omega = 10$		
$\nu_{\text{probe}}$ (cm <sup>-1</sup> )	$T_1$ (ps)	$T_r$ (ps)	$\nu_{\text{probe}}$ (cm <sup>-1</sup> )	$T_1$ (ps)	$T_r$ (ps)	$\nu_{\text{probe}}$ (cm <sup>-1</sup> )	$T_1$ (ps)	$T_r$ (ps)	$\nu_{\text{probe}}$ (cm <sup>-1</sup> )	$T_1$ (ps)	$T_r$ (ps)
1840	31 ± 2		1850	24 ± 3		1860	22 ± 2		1868	16 ± 2	
1850	39 ± 2		1860	29 ± 1		1870	22 ± 2		1875	18 ± 2	
1860	42 ± 2		1870	28 ± 2		1880	21 ± 2		1882	18 ± 2	
1880	41 ± 2		1890	29 ± 2		1900	23 ± 2		1890	16 ± 2	
1890	37 ± 2		1900	25 ± 1	>150	1910	19 ± 1	>100	1907	19 ± 1	
1900	32 ± 2		1910	22 ± 1	>150	1920	15 ± 1	>100	1915	16 ± 1	
1910	33 ± 4	>180	1920	19 ± 2		1930	12 ± 2		1923	13 ± 1	>100
									1930	12 ± 2	>100
bulk H <sub>2</sub> O <sup>a</sup>	7.3 ± 0.8	16 ± 5							1938	12 ± 2	

<sup>a</sup> Data from ref 57.

precludes identifying any significant trends in the results with respect to the effect of the RM environment. For bulk solution, a larger solvent dependence was seen for  $T_r$  than  $T_1$ . This suggests that  $T_r$  times may be more useful in establishing the effects of RM confinement than the  $T_1$  times, but the large uncertainties and lack of obvious trends, combined with the lack of knowledge of how the dipolar reorientation mechanism should depend on solvent properties, precludes definite conclusions based on the  $T_r$  times.

The trends in IR band peak positions of ferricyanide as a function of surfactant and  $\omega$  and are easier to see and to interpret in terms of solute location. For anionic AOT RMs, the IR band positions are the same as in bulk water for all values of  $\omega$ . The largest shift from the bulk value is seen for cationic CTAB RMs, in which the shift initially decreases as  $\omega$  increases but then remains nearly constant for  $\omega \geq 5$ . For the nonionic RMs, the IR band is shifted to the red and then approaches the bulk value as  $\omega$  increases. The shifts from the bulk are larger for NP RMs than for Brij-30 RMs. These results are similar to what was observed for azide, where the most bulklike environment was seen when solute and surfactant charges were the same. The least bulklike environment was seen for oppositely charged solute and surfactant where the behavior reached a plateau and further increases in  $\omega$  made little or no difference in the behavior of the system. Intermediate behavior was seen for the nonionic surfactant with the shorter chain Brij-30 behaving more like bulk water. Unfortunately, this behavior is not revealed in the dynamics of ferricyanide, with the exception of slightly slower dynamics in CTAB RMs. When compared to bulk solvent behavior, CTAB RMs show a larger peak shift than seen for ethylene glycol ( $\sim 4$  cm<sup>-1</sup> vs  $\sim 2$  cm<sup>-1</sup>). However, there is little change in  $T_r$  in CTAB RMs whereas  $T_1$  doubled in going from H<sub>2</sub>O to ethylene glycol. For NP, the peak shift is similar or greater than in ethylene glycol, but again no change in  $T_r$  is observed.

**SNP.** The  $T_1$  times for the NO band of SNP in AOT RMs are within the uncertainty of the bulk water  $T_1$  time.<sup>57</sup> This suggests that SNP resides in a bulklike region in the center of the RM water pool. This is what would be expected on the basis of the Coulombic repulsion between the SNP anion and the anionic headgroups of AOT. However, the  $T_r$  times, which correspond to the molecular reorientation times, are longer than the bulk value by a factor of 2–3. This is not unexpected because the translational mobility of water should be reduced even in the center of the RM water pool for relatively small RMs. Similarly, for azide in AOT RMs, the  $T_1$  times were indistinguishable from the bulk values in all cases.<sup>51</sup> The  $T_r$  times were also indistinguishable from the bulk for  $\omega$  of 10 or more, but  $T_r$  was longer for the smallest RM studied,  $\omega = 5$ .<sup>51</sup> In the case of the SNP solute,  $T_r$  is longer for both cases studied,  $\omega = 6$  and 7. This is not surprising because SNP is a larger anion

than azide and should have a larger solvation shell. This larger solvation shell should experience a reduction in mobility and an increase in  $T_r$  times for larger RMs than the solvation shell of azide. The water pool radii are  $\sim 20$  Å with 500–1000 water molecules per RM.<sup>31,68</sup> The size of the pool of free water is apparently large enough ( $\sim 10$  Å)<sup>13,31,67</sup> to result in a solvent environment that appears bulklike to the VER dynamics of SNP with a  $\sim 3.5$  Å radius, but small enough to restrict the mobility of the larger solvation shell enough to slow molecular reorientation. The static spectral behavior is also similar to azide. The IR band is blue shifted from the bulk, the opposite of what is seen for the other RMs. A red shift is to be expected if SNP is in a less polar solvation environment, as occurs in the other RMs, suggesting that SNP resides in a bulklike region of the water pool. The small blue shift may be attributed to the high concentration of Na<sup>+</sup> counterions from the AOT surfactant. Supporting evidence for this interpretation was found in our observation that addition of NaCl to an aqueous solution of SNP induces a blue shift in the IR band of up to 3 cm<sup>-1</sup> for a solution that is nearly saturated with SNP and NaCl.

For SNP in CTAB RMs, both  $T_1$  and  $T_r$  are longer by a factor of 6–7. As  $\omega$  is increased,  $T_1$  decreases but does not approach the bulk value. This is consistent with a strong interaction with the wall due to the Coulombic attraction between the SNP anion and the cationic CTAB headgroups. The  $\omega$  dependence of the  $T_1$  time could be due to a change in the properties of the water solvating one side of SNP. The radii of the RM interior is on the order of 15 Å with  $\sim 500$  water molecules per RM.<sup>16</sup> The bound layer in CTAB RMs is approximately 10 Å thick,<sup>12,13,16</sup> suggesting that the  $\sim 7$  Å diameter SNP ion may have some interaction with the bulk water pool. The  $T_r$  time either remains the same or increases as  $\omega$  increases, but the large uncertainties prevent distinguishing between these possibilities. This is also consistent with a strong interaction with the micelle wall. However, the measured  $T_r$  times are not consistent with the rotation times of the entire micelle, which are on the order of 1 ns.<sup>36,37,73</sup> This could imply that SNP is restricted to the outer water layer rather than directly attached to the micelle wall. Attachment to the micelle wall is still possible if the attachment only restricts the amount of reorientation without preventing it altogether. Our data cannot distinguish between these two possibilities because the  $T_r$  times are longer than the  $T_1$  times and the complete anisotropy decay cannot be followed in our experiment. Regardless of the exact mechanism, the results indicate a strong interaction between the SNP anion and the CTAB cation. Similar behavior was also seen for azide in CTAB RMs. These results are reminiscent of results seen for hydrophobic probes where the probes also reside in the interfacial region of the RM.<sup>28,54</sup> The static spectral behavior is also consistent with a strong interaction with the interface. For all  $\omega$ , the IR band is red shifted significantly, at least 27 cm<sup>-1</sup>

from the bulk, indicating an environment significantly different than bulk water. In addition, the red shift does not change much with  $\omega$ , decreasing by less than  $2\text{ cm}^{-1}$  between  $\omega = 2$  and  $\omega = 4$  and remaining constant as  $\omega$  is increased further. This indicates a solvation environment that changes little as the RM size is increased, which would be expected for a probe located at or near the micelle wall. Although the Coulomb effects between the probe and surfactant present an attractive, simple explanation, the presence of counterions may complicate this interpretation. Simulations of AOT RMs<sup>30,31,74</sup> predict that the counterions are mostly associated with or near the headgroups with only  $\sim 10\text{--}30\%$  of the counterions in the free region of the water pool. This suggests the possibility that the presence of counterions near the headgroups may shield the effect of the Coulomb attraction between the surfactant headgroups and the probe and possibly overwhelm that interaction. However, the most straightforward interpretation of our results as well as results from a previous MD simulation<sup>32</sup> is consistent with a Coulomb attraction between the headgroups and probes, suggesting that the counterions do not eliminate the Coulombic interactions, although they may have an effect on the strength of the interactions. The most apparent consequence of the counterions is the blue-shift from bulk water in AOT RMs for the NO band of SNP and as previously reported<sup>20</sup> for azide.

In both NP and Brij-30 RMs, SNP has an IR absorption band that is much broader than in bulk water or in ionic CTAB and AOT RMs. In Brij-30 RMs the IR band appears to exhibit a second unresolved peak. Addition of azide to SNP containing RMs resulted in azide IR bands that were identical to those in SNP free RMs,<sup>51</sup> suggesting that the RM structure is unchanged by the presence of SNP. The NP RM sizes range from  $13\text{ \AA}$  ( $\omega = 3$ ) to  $35\text{ \AA}$  ( $\omega = 10$ ) with  $\sim 300$  to  $\sim 5000$  water molecules, although these size data probably include the poly-oxo chain containing regions.<sup>20</sup> It is tempting to describe the SNP results in terms of two species, those in the water pool and those in the poly-oxo chains containing region. This is especially tempting due to the spectral shape changes in Figure 8, where a new band appears to grow in upon the addition of water that is closer in frequency to the bulk water band. This is also consistent with previous studies that suggest a water pool does not form until  $\omega$  is large enough.<sup>28,33,70</sup> However, the  $T_1$  and  $T_r$  times are probe frequency dependent in a continuous manner. Even though the static spectra of SNP in Brij-30 RMs appear to have two bands, the time-resolved data are not consistent with a two-site model. For both nonionic RM systems, attempts to fit the transient decays to two or more exponentials were no better than with a single time constant. Although the water molecules may reside in two regions, within the poly-oxo chains and in water pools, the interface between the regions is poorly defined. The poorly defined interface and the frequency dependence of the VER rates suggest that SNP occupies a continuous range of solvation environments rather than a small number of discrete solvation environments. The  $T_1$  times appear to be shorter on the blue side of the static absorption band in both RM systems. This behavior reflects a solvation environment with weaker solute solvent interactions than bulk water causing both a red shift in the static absorption band and an increase in the  $T_1$  time as has been seen for other RM systems. For both RM systems, the  $T_1$  times get shorter with increasing  $\omega$ . In addition, the surfactant with the longer poly-oxo chain, NP, has longer  $T_1$  times and spectra that are shifted farther to the red. For  $\omega = 10$  Brij-30, the  $T_1$  times from the blue edge of the static absorption, closest in frequency to the bulk, are within the uncertainty of the bulk, whereas the  $T_1$  times in NP remain

longer than in the bulk in all cases. The  $T_r$  times in Brij-30 RMs also show a significant frequency dependence, but they remain too long to measure in all cases for NP. For Brij-30, the  $T_r$  times are shorter in the more blue regions and are generally faster for larger  $\omega$ . This is similar to the trends seen for the  $T_1$  times, but the  $T_r$  times do not reach the bulk value.

The smaller red shift and faster dynamics seen for Brij-30 RMs suggest that the micelle interior has a more bulklike region than the NP RMs. This is consistent with the structure of the nonionic surfactants, where Brij-30 has shorter poly-oxo chains. These shorter chains should be fully solvated at smaller  $\omega$ , allowing the formation of a water pool at smaller  $\omega$  than is possible with NP. Similar behavior was seen in azide.<sup>51</sup> However, it is obvious that SNP resides in some regions of the RM interior that differ greatly from bulk water. Even for the largest Brij-30 RMs the  $T_1$  and  $T_r$  times measured in the transient absorption region to the red of the static absorption are much longer than in bulk water. This frequency dependent behavior was not seen for azide or for the hexacyanoferrates. This is likely related to the solubility characteristics of SNP. Unlike the hexacyanoferrates, SNP has a smaller charge and is soluble in methanol and bulk TGE. SNP is also soluble in less polar solvents than the sodium salt of azide. This increases the likelihood of a favorable interaction between the poly-oxo chains and the SNP molecule. Rather than preferring the most polar solvation environment available, as was seen for azide and hexacyanoferrates, SNP appears to have little preference between residing in the most polar region of the water pool or within the poly-oxo chains. This is unlike the ionic RMs in which the location of the anions is primarily determined by Coulombic interactions, resulting in similar behavior for all three cyanoferrates.

Experiments in  $\text{H}_2\text{O}/\text{TGE}$  mixtures, meant to model the regions containing poly-oxo chain of the nonionic RMs, reveal somewhat different behavior for SNP than seen in the RMs. The  $T_1$  times in the  $\text{H}_2\text{O}/\text{TGE}$  mixtures also show a probe frequency dependence with faster rates to the blue, but the frequency dependence is much weaker than in the nonionic RMs and is similar to bulk TGE. Overall, the times are similar in the mixtures and in the RMs for a given  $\omega$ , but the  $T_1$  times do not come as close to the bulk value in the bluest regions. Although the static absorption bands are broader than bulk water, they are much narrower than in the nonionic RMs and similar to bulk TGE in width. These results suggest that there is greater segregation of water and the poly-oxo chains in the nonionic RMs than the  $\text{H}_2\text{O}/\text{TGE}$  mixtures. This suggests that there is an inhomogeneous distribution of solvation sites in the nonionic RMs, unlike the  $\text{H}_2\text{O}/\text{TGE}$  mixtures that have a much more uniform solvent distribution. Any inhomogeneities in the  $\text{H}_2\text{O}/\text{TGE}$  mixtures are similar to those in bulk TGE. This is also supported by the  $T_r$  trends.  $T_r$  is relatively short only in larger Brij-30 RMs when probed in the high-frequency region. Similar segregation to form water pools was inferred for azide on the basis of chain length vs rate comparisons. However, the results here are much clearer due to the inhomogeneous distribution of SNP in the nonionic RMs.

## Conclusion

We have performed VER measurements on a series of cyanoferrates in cationic, anionic, and nonionic reverse micelles. The cyanoferrates studied are ferrocyanide  $[\text{Fe}(\text{CN})_6^{4-}]$ , ferricyanide  $[\text{Fe}(\text{CN})_6^{3-}]$ , and sodium nitroprusside  $[\text{SNP}, \text{Fe}(\text{CN})_5\text{NO}^{2-}]$ . These results have been compared to dynamics in bulk aqueous solution and are interpreted in terms of the

location of the cyanoferrate probes within the RM cavity. For ferrocyanide, which forms stable solutions in anionic AOT and nonionic Brij-30 RMs, the VER dynamics were indistinguishable from the bulk in all cases. The same was seen for the anisotropy decay, in this case due to dipolar reorientation of the transition dipole by exchange between degenerate modes. Based on the previously observed large solvent dependence of the VER rate, our data suggest that ferrocyanide resides in a bulklike water pool in the RM core. The results for ferrocyanide in Brij-30 are also indistinguishable from those in bulk water, suggesting that the high charge on the ferrocyanide ion leads to a strong preference for solvation by water molecules rather than within the poly-oxo chains. For ferricyanide, VER dynamics in nonionic NP and Brij-30 RMs were indistinguishable from bulk water whereas a slight reduction in VER rate was measured in cationic CTAB RMs. The anisotropy decays were again due to the dipolar reorientation mechanism and were indistinguishable from the bulk. Due to the small dependence of the VER dynamics on bulk solvent or RM properties, the static spectral shifts observed lead to a more clear dependence on surfactant charge. The largest shifts from the bulk were seen for cationic CTAB and no shift was observed for AOT. The nonionic RMs show an intermediate shift with a larger shift seen for the surfactant with the longer poly-oxo chain, NP.

The largest variation in VER dynamics with surfactant charge was seen for SNP, in part because it was stable in the most RMs. VER dynamics were indistinguishable from the bulk in AOT RMs and the anisotropy decays were slowed by a factor of less than 3. In CTAB RMs, both  $T_1$  and  $T_2$  were slowed by a factor of 6–7. In the nonionic RMs, the VER dynamics of SNP had a dependence on probe frequency with faster dynamics in the higher frequency region. The VER rate also generally increases with  $\omega$ . The anisotropy decay, corresponding to molecular reorientation, shows a similar dependence on frequency and  $\omega$  for Brij-30 RMs but remains too long to measure in NP RMs. The results suggest that SNP resides in a bulklike region in the center of the water core due to Coulombic repulsion in AOT RMs and strongly interacts with the oppositely charged micelle wall in CTAB RMs. For the nonionic RMs, there is a range of sites in which SNP can reside, differing in water content, resulting in frequency dependent dynamics. These results are consistent with the static spectra, which for the nonionic RMs are very broad and significantly red shifted from the bulk with a significant dependence on  $\omega$ . For AOT, the static spectra show a small blue shift compared to the bulk, whereas in CTAB RMs SNP shows a large, relatively  $\omega$  independent red shift.

The effects of confinement on both the location and dynamics of a probe appear to depend on the relative charge of the probe and the confining system when both are charged. The results of this study show that the vibrational spectra and dynamics of anionic probes closely resemble that in bulk water in AOT RMs in which the surfactant headgroup is also negatively charged. This suggests that the anions reside in a more bulklike environment, which is most likely in the center of the RM core due to Coulombic repulsion with the surfactant headgroup. Conversely, for cationic CTAB, there is a strong attraction between the surfactant and anion probe, resulting in an environment differing from the bulk with a small dependence on RM size. In nonionic RMs, the location of the probe depends on the nature of the probe. A more hydrophilic probe results in a more bulklike the solvation environment. These results are similar to previous studies of azide in RMs of differing charge. The results of this study demonstrate that confinement effects

on ions in RMs and probably other related interfacial systems are strongly affected by the relative charge between the ion and the interface.

**Acknowledgment.** Support for this work was provided by the Office of Naval Research through the Naval Research Laboratory. G.M.S. acknowledges the Naval Research Laboratory–American Society for Engineering Education Postdoctoral Fellowship program. K.D. acknowledges the Naval Research Laboratory–National Research Council Research Associateship.

## References and Notes

- (1) Weik, M. *Eur. Phys. J. E* **2003**, *12*, 153.
- (2) Bellissent-Funel, M. C. *J. Phys.: Condens. Matter* **2001**, *13*, 9165.
- (3) Nandi, N.; Bhattacharyya, K.; Bagchi, B. *Chem. Rev.* **2000**, *100*, 2013.
- (4) Scodinu, A.; Fourkas, J. T. *J. Phys. Chem. B* **2002**, *106*, 10292.
- (5) Hazra, P.; Chakrabarty, D.; Chakraborty, A.; Sarkar, N. *Chem. Phys. Lett.* **2004**, *388*, 150.
- (6) Bellissent-Funel, M. C. *Eur. Phys. J. E* **2003**, *12*, 83.
- (7) Rovere, M.; Gallo, P. *Eur. Phys. J. E* **2003**, *12*, 77.
- (8) Douhal, A. *Chem. Rev.* **2004**, *104*, 1955.
- (9) Bhattacharyya, K.; Bagchi, B. *J. Phys. Chem. A* **2000**, *104*, 10603.
- (10) Li, S.; Shepard, T. D.; Thompson, W. H. *J. Phys. Chem. A* **2004**, *108*, 7347.
- (11) Bohidar, H. B.; Behboudnia, M. *Colloids Surf., A* **2001**, *178*, 313.
- (12) Das, P. K.; Chaudhuri, A.; Saha, S.; Samanta, A. *Langmuir* **1999**, *15*, 4765.
- (13) Giustini, M.; Palazzo, G.; Colafemmina, G.; DellaMonica, M.; Giomini, M.; Ceglie, A. *J. Phys. Chem.* **1996**, *100*, 3190.
- (14) Petit, C.; Bommaris, A. S.; Pileni, M. P.; Hatton, T. A. *J. Phys. Chem.* **1992**, *96*, 4653.
- (15) Lang, J.; Jada, A.; Malliaris, A. *J. Phys. Chem.* **1988**, *92*, 1946.
- (16) Lang, J.; Mascolo, G.; Zana, R.; Luisi, P. L. *J. Phys. Chem.* **1990**, *94*, 3069.
- (17) Griffiths, P. C.; Cheung, A. Y. F.; Farley, C.; Paul, A.; Heenan, R. K.; King, S. M.; Pettersson, E.; Stilbs, P.; Ranganathan, R. *J. Phys. Chem. B* **2004**, *108*, 1351.
- (18) Griffiths, P. C.; Paul, A.; Heenan, R. K.; Penfold, J.; Ranganathan, R.; Bales, B. L. *J. Phys. Chem. B* **2004**, *108*, 3810.
- (19) Vasilescu, M.; Caragheorghopol, A.; Caldararu, H. *Adv. Colloid Interface Sci.* **2001**, *89*, 169.
- (20) Zhong, Q.; Steinhurst, D. A.; Carpenter, E. E.; Owrutsky, J. C. *Langmuir* **2002**, *18*, 7401.
- (21) Onori, G.; Santucci, A. *J. Phys. Chem.* **1993**, *97*, 5430.
- (22) Brubach, J. B.; Mermet, A.; Filabozzi, A.; Gerschel, A.; Lairez, D.; Krafft, M. P.; Roy, P. *J. Phys. Chem. B* **2001**, *105*, 430.
- (23) Jain, T. K.; Varshney, M.; Maitra, A. *J. Phys. Chem.* **1989**, *93*, 7409.
- (24) Macdonald, H.; Bedwell, B.; Gulari, E. *Langmuir* **1986**, *2*, 704.
- (25) Venables, D. S.; Huang, K.; Schmittenmaer, C. A. *J. Phys. Chem. B* **2001**, *105*, 9132.
- (26) Gonzalez-Blanco, C.; Rodriguez, L. J.; Velazquez, M. M. *J. Colloid Interface Sci.* **1999**, *211*, 380.
- (27) Correa, N. M.; Biasutti, M. A.; Silber, J. J. *J. Colloid Interface Sci.* **1996**, *184*, 570.
- (28) Qi, L. M.; Ma, J. M. *J. Colloid Interface Sci.* **1998**, *197*, 36.
- (29) Kawai, T.; Shindo, N.; Konno, K. *Colloid Polym. Sci.* **1995**, *273*, 195.
- (30) Faeder, J.; Albert, M. V.; Ladanyi, B. M. *Langmuir* **2003**, *19*, 2514.
- (31) Faeder, J.; Ladanyi, B. M. *J. Phys. Chem. B* **2000**, *104*, 1033.
- (32) Faeder, J.; Ladanyi, B. M. *J. Phys. Chem. B* **2001**, *105*, 11148.
- (33) Allen, R.; Bandyopadhyay, S.; Klein, M. L. *Langmuir* **2000**, *16*, 10547.
- (34) Brown, D.; Clarke, J. H. R. *J. Phys. Chem.* **1988**, *92*, 2881.
- (35) Corbeil, E. M.; Levinger, N. E. *Langmuir* **2003**, *19*, 7264.
- (36) Pant, D.; Levinger, N. E. *Langmuir* **2000**, *16*, 10123.
- (37) Riter, R. E.; Willard, D. M.; Levinger, N. E. *J. Phys. Chem. B* **1998**, *102*, 2705.
- (38) Levinger, N. E. *Curr. Opin. Colloid Interface Sci.* **2000**, *5*, 118.
- (39) Hazra, P.; Sarkar, N. *Chem. Phys. Lett.* **2001**, *342*, 303.
- (40) Mandal, D.; Pal, S. K.; Datta, A.; Bhattacharyya, K. *Anal. Sci.* **1998**, *14*, 199.
- (41) Datta, A.; Mandal, D.; Pal, S. K.; Bhattacharyya, K. *J. Phys. Chem. B* **1997**, *101*, 10221.
- (42) Jiang, Y. B.; Jin, M. G. *Spectrochim. Acta, Part A* **2000**, *56*, 623.
- (43) Vinogradov, A. M.; Tatikolov, A. S.; Costa, S. M. B. *Phys. Chem. Chem. Phys.* **2001**, *3*, 4325.



- (44) Datta, A.; Mandal, D.; Pal, S. K.; Bhattacharyya, K. *Chem. Phys. Lett.* **1997**, 278, 77.
- (45) Fioretto, D.; Freda, M.; Mannaioli, S.; Onori, G.; Santucci, A. *J. Phys. Chem. B* **1999**, 103, 2631.
- (46) Mittleman, D. M.; Nuss, M. C.; Colvin, V. L. *Chem. Phys. Lett.* **1997**, 275, 332.
- (47) Patzlaff, T.; Janich, M.; Seifert, G.; Graener, H. *Chem. Phys.* **2000**, 261, 381.
- (48) Seifert, G.; Patzlaff, T.; Graener, H. *Phys. Rev. Lett.* **2002**, 88, 147402.
- (49) Zhong, Q.; Baronavski, A. P.; Owrutsky, J. C. *J. Chem. Phys.* **2003**, 119, 9171.
- (50) Zhong, Q.; Baronavski, A. P.; Owrutsky, J. C. *J. Chem. Phys.* **2003**, 118, 7074.
- (51) Sando, G. M.; Dahl, K.; Owrutsky, J. C. *J. Phys. Chem. A* **2004**, 11, 209–11 217.
- (52) Rack, J. J.; McCleskey, T. M.; Birnbaum, E. R. *J. Phys. Chem. B* **2002**, 106, 632.
- (53) Saez, M.; Abuin, E. A.; Lissi, E. A. *Langmuir* **1989**, 5, 942.
- (54) Hazra, P.; Chakrabarty, D.; Chakraborty, A.; Sarkar, N. *Chem. Phys. Lett.* **2003**, 382, 71.
- (55) Ohta, K.; Maekawa, H.; Tominaga, K. *J. Phys. Chem. A* **2004**, 108, 1333.
- (56) Ohta, K.; Maekawa, H.; Tominaga, K. *Chem. Phys. Lett.* **2004**, 386, 32.
- (57) Sando, G. M.; Zhong, Q.; Owrutsky, J. C. *J. Chem. Phys.* **2004**, 121, 2158.
- (58) Tokmakoff, A.; Fayer, M. D. *Acc. Chem. Res.* **1995**, 28, 437.
- (59) Tokmakoff, A.; Fayer, M. D. *J. Chem. Phys.* **1995**, 103, 2810.
- (60) Childs, J.; Beckerle, J. D. *J. Chem. Phys.* **1997**, 107, 319.
- (61) Heilweil, E. J.; Casassa, M. P.; Cavanagh, R. R.; Stephenson, J. C. *Annu. Rev. Phys. Chem.* **1989**, 40, 143.
- (62) Heilweil, E. J.; Cavanagh, R. R.; Stephenson, J. C. *Chem. Phys. Lett.* **1987**, 134, 181.
- (63) Owrutsky, J. C.; Kim, Y. R.; Li, M.; Sarisky, M. J.; Hochstrasser, R. M. *Chem. Phys. Lett.* **1991**, 184, 368.
- (64) Li, M.; Owrutsky, J.; Sarisky, M.; Culver, J. P.; Yodh, A.; Hochstrasser, R. M. *J. Chem. Phys.* **1993**, 98, 5499.
- (65) Dahl, K.; Sando, G. M.; Owrutsky, J. Manuscript in preparation.
- (66) Estrin, D. A.; Baraldo, L. M.; Slep, L. D.; Barja, B. C.; Olabe, J. A.; Paglieri, L.; Corongiu, G. *Inorg. Chem.* **1996**, 35, 3897.
- (67) Maitra, A. *J. Phys. Chem.* **1984**, 88, 5122.
- (68) Gehlen, M. H.; Deschryver, F. C. *Chem. Rev.* **1993**, 93, 199.
- (69) Caldararu, H.; Caragheorgheopol, A.; Vasilescu, M.; Dragutan, I.; Lemmetyinen, H. *J. Phys. Chem.* **1994**, 98, 5320.
- (70) Dutt, G. B. *J. Phys. Chem. B* **2004**, 108, 7944.
- (71) Kimura, N.; Umemura, J.; Hayashi, S. *J. Colloid Interface Sci.* **1996**, 182, 356.
- (72) Sando, G. M.; Owrutsky, J. C. Unpublished results.
- (73) Krishnakumar, S.; Somasundaran, P. *J. Colloid Interface Sci.* **1994**, 162, 425.
- (74) Abel, S.; Sterpone, F.; Bandyopadhyay, S.; Marchi, M. *J. Phys. Chem. B* **2004**, 108, 19458.